Atomic layer deposited ZnO:Al for nanostructured silicon heterojunction solar cells

M. Steglich[a,1] , A. Bingel[b], G. Jia[a], F. Falk[a]

[a]Institute of Photonic Technology, Albert-Einstein-Str. 9, 07745 Jena, Germany
[b]Fraunhofer Institute for Applied Optics and Precision Engineering, Albert-Einstein-Str. 7, 07745 Jena, Germany

Abstract

For transparent front contacts of nanostructured silicon solar cells aluminum doped zinc oxide (ZnO:Al), deposited by atomic layer deposition (ALD), is investigated. For this purpose it is crucial that the ZnO:Al layer covers the nanostructures conformally. ZnO:Al deposition at a temperature of 225°C, compatible with the underlying solar cell structures, yields a resistivity of $1.2 \cdot 10^{-3}$ Ωcm and 85% mean optical transmittance in the VIS-NIR range (< 1300 nm). The complex dielectric function of the ALD-ZnO:Al is determined by fitting optical spectra with a multi-oscillator model. An investigation of the layer structure shows a preferential growth in the c-direction of the hexagonal ZnO crystal and 100-200 nm long wedge-shaped crystallites. I-V measurements on planar ZnO:Al/a-Si:H(n/p)/c-Si(n^+/p^+) test structures reveal the nature of the ZnO:Al contact to both n- and p-type a-Si:H. Simple planar solar cells exhibited an excellent rectification behaviour and open circuit voltages $V_{OC} = 620 \ldots 640$ mV.
The feasibility of nanostructure silicon heterojunction solar cells is demonstrated by showing the conformal coating of deep Si nanowire structures.

Keywords: Silicon heterojunction; Atomic layer deposition; ZnO:Al; Black Silicon; Nanowire; Nanostructure

1. Introduction

For realizing silicon solar cells competitive to conventional energy sources, reducing the costs per Watt solar power ($/$W_P$) is crucial. The use of crystalline silicon thin films on glass and thus lowered material costs could be a way to achieve this aim [1].
Due to the relatively low absorption of crystalline silicon in the VIS/NIR spectral region, such solar cells rely on a perfect light trapping regime which can be realized by structuring the films. A nanostructure with high aspect ratio, so-called “Black Silicon”, fabricated by vapour-liquid-solid (VLS) [2, 3], wet [4, 5] or dry etching techniques [6] is a potential low-cost surface modification leading to excellent light-trapping. Using a nanowire structure, a promising cell concept (see Fig. 1) utilizes a hydrogenated, amorphous silicon heteroemitter, which on the one hand is able to lower the carrier recombination at the front surface [7]. On

[1] Corresponding author. Present address: Institute of Applied Physics, Albert-Einstein-Str. 15, 07745 Jena, Germany. Tel.: +49 3641 947838. Fax: +49 3641 947802.
E-mail address: martin.steglich@uni-jena.de

the other hand it can easily be deposited uniformly by a PECVD process. However, amorphous silicon exhibits a rather low conductivity and therefore has to be coated with a transparent front electrode, lowering the series resistance of the solar cell and ensuring ohmic contact to the emitter.
Since this electrode has to be deposited homogenously and uniformly on a nanostructure with high aspect ratio, a useful preparation technique is Atomic Layer Deposition (ALD) of Al-doped zinc oxide (ZnO:Al or AZO) [8, 9].
Utilizing thermal ALD, layers of intrinsic ZnO can be built up by alternate pulses of diethylzinc (DEZ) and water at a sufficient reactor temperature. For an additional doping with Al, single DEZ pulses are substituted by pulses of trimethylaluminium (TMA), leading to the deposition of an Al_2O_3 monolayer [8]. Hence, there are basically only two critical parameters: Al doping, i.e. the ratio between DEZ and TMA pulses N_{DEZ} / N_{TMA}, and substrate temperature T.
This article demonstrates that ZnO:Al thin films prepared by ALD cover nanostructured silicon heterojunction solar cells conformally. The film properties at different deposition conditions were analyzed. For a determination of the contact properties to a-Si:H the films were prepared on silicon wafers covered by a-Si:H, that is a flat heterojunction solar cell configuration. Finally, highly conformal ZnO:Al films were deposited on nanowire solar cell structures.

2. Experimental

Transparent, conductive ZnO:Al films were deposited from the precursor gases diethylzinc (DEZ), trimethylaluminium (TMA) and water onto borosilicate glass substrates (Schott Boro33, 1"x1") using a Beneq TFS 200. Prior to the deposition the base pressure was kept at 2 mbar of N_2. The glass substrates were cleaned with ethanol before placing them into the deposition chamber. The chamber was continuously purged with 100 to 200 sccm N_2. During deposition it was heated to temperatures ranging from 150 °C to 300 °C in order to assure thermal decomposition of the precursors. The used precursor pulse length of 100 ms was sufficient for a homogenous deposition. After each pulse the reaction chamber was purged with pure N_2 for 350 ms to remove unreacted precursors.
For resistivity measurements a four-point in-line tip configuration was applied. Film thicknesses were determined by fitting a single-layer multi-oscillator model (9 oscillators) for the dielectric function ε to measured transmittance and reflectance spectra (see 3.2). UV-NIR spectra were taken using a PerkinElmer Lambda 950 spectrometer. Carrier density n and mobility μ was determined by Hall measurements using van-der-Pauw geometry. Layer composition was measured via energy dispersive X-ray spectroscopy (EDS).
For contact measurements and solar cell fabrication Si wafers were RCA cleaned and dipped in diluted HF (2%) for 2 min to remove the native silicon oxide. Immediately after etching the wafers were transferred into a parallel-plate PECVD chamber for the deposition of thin a-Si:H layers. The deposition was carried out at a reactor pressure of 0.5 mbar with a silane flow of 2 sccm, a helium flow of 15 sccm, and a doping gas flow of 1 sccm (2% PH_3 in He for n-type doping or 2% B_2H_6 in He for p-type doping). Before the ALD of the front electrode, the samples were again dipped in diluted HF. Back contacts on c-Si(n) were fabricated by sputtering of Cr.

3. Results and Discussion

3.1. Electrical characterization

Fig. 2 illustrates the specific resistivity $\rho = e \cdot n \cdot \mu$ (e…elementary charge, μ…carrier mobility) of ZnO:Al layers for various deposition conditions. Film thicknesses ranged mostly from 100 to 150 nm, while only few samples were thicker (around 300 nm). A notable dependence of resistivity on film thickness was not observed.

Obviously, the optimal ratio of pulses of DEZ and TMA N_{DEZ} / N_{TMA} with regard to conductivity amounts to about 20:1, in agreement with the results of other authors [10, 11]. In the substrate temperature range below 200°C, the specific resistivity declines rapidly with increasing temperature, while for $T > 200°C$ it shows only a slight decrease with substrate temperature.

An explanation for this behavior is given in Fig. 3. While for $N_{DEZ} / N_{TMA} = 20:1$ the carrier density grows with temperature and finally saturates around 275°C, the carrier mobility reaches a maximum at about 225°C and then slowly falls off, which nearly compensates the carrier density improvement.

Starting from high N_{DEZ} / N_{TMA}, for a given temperature the carrier density increases with adding more TMA/water cycles until N_{DEZ} / N_{TMA} reaches a ratio of 10:1. On the other hand, for $T \geq 200°C$, the mobility declines and finally drops heavily for $N_{DEZ} / N_{TMA} = 10:1$.

For a 20:1 cycle ratio a distinct maximum value of the mobility occurs at 225°C. In order to clarify the origin of this mobility maximum, additional EDS measurements were performed to distinguish between Al concentration c_{Al} and effective Al doping (Fig. 4a).

The Al concentration in the layers shows the expected behavior, i.e. an increase with decreasing cycle ratio. Furthermore, a slight dip in the curves at around 175-200°C is apparent. This may be explained as result of the different temperature dependencies of the ZnO and Al_2O_3 growth rates $\dot{d}$ that are sketched in Fig. 4b: The depicted deposition rate for ZnO was measured separately; the one for Al_2O_3 is taken from [12]. The latter exhibits a slight decrease of the growth rate with temperature which is typical for the thermal ALD of Al_2O_3 from TMA and water. This behaviour results from the reduced surface concentration of OH groups with rising temperature and has been shown both for alumina and silica surfaces [13]. Since the density of OH groups on a ZnO surface is believed to decrease with temperature, too [14,15], we assume that the growth rate dependence for single Al_2O_3 monolayers on a ZnO surface does not differ qualitatively from that on an Al_2O_3 or silica surface. Hence, it is possible to assess the principle curve shape of $c_{Al}(T)$ by calculating the rate ratio (N_i…atomic density of element i)

$$c_{Al} = \frac{N_{Al}}{N_{Al} + N_{Zn} + N_O} \approx \frac{N_{Al}}{2N_{Zn}} \sim \frac{\dot{d}_{Al}}{\dot{d}_{Zn}}$$

since $N_{Al} << N_{Zn} \approx N_O$. This estimation, represented by the solid line in Fig. 4, shows a minimum around 175-200 °C and hence agrees well with the experiment.

The EDS data were also used to calculate the doping efficiency, neglecting the self-doping of intrinsic ZnO (Fig. 5). For that purpose, the carrier densities of the 20:1 samples were divided by the Al density of the according layer, assuming a ZnO bulk atomic density of $8.87 \cdot 10^{22}$ cm^{-3}. The resulting doping efficiency yields a maximum at 225°C, just like the mobility behavior of the corresponding samples. This means that at a certain temperature an increase in Al concentration is not fully accompanied by an increase in carrier density. In fact, there is a growing amount of excess Al that does not arrange substitutionally in the ZnO lattice but remains as Al_2O_3 precipitate. Those precipitates would then act as scattering centres for the electrons and therefore lower the carrier mobility [16] as observed in our experiments. This mechanism of mobility increase has also been observed by others for CVD and ALD deposition techniques [17, 30] as well as for sputtering [18, 19].

Concerning the utilization of ZnO:Al layers as front electrodes in a-Si:H/c-Si heterojunction solar cells, it is important to state that low resistivities around 10^{-3} Ωcm can already be achieved at $T < 250°C$, i.e. at temperatures low enough to avoid considerable hydrogen effusion out of the amorphous silicon [20]. Otherwise the fabrication of the transparent front contact itself could degrade the passivation properties of the a-Si:H [21, 22, 23] and hence limit the performance of the solar cell.
On the other hand, an application of a TCO in a silicon heterojunction solar cell typically requires a resistance well below 100 Ω/sq at a layer thickness of 80 to 90 nm (in order to serve as an antireflection coating). This can obviously not be achieved with the best presented resistivity of about 10^{-3} Ωcm. Hence, with regard to nanostructure silicon heterojunction solar cells, we propose to combine an Atomic Layer Deposition of a thin ZnO:Al layer with a state-of-the-art TCO film obtained by another, more common deposition technique like magnetron sputtering. Then, the ALD-ZnO:Al would provide the necessary conformal contact to the amorphous emitter, while the second TCO film - with a considerably lower resistivity of the order of 10^{-4} Ωcm [16,24,25] – would assure a sufficient lateral conductivity with a sheet resistance below 100 Ω/sq. Moreover, this should be more cost-efficient on an industrial scale, since deposition rates in a pure ALD process are rather low compared to, for example, a sputtering process.

3.2. Optical characterization

UV-VIS spectra were taken to evaluate the thickness and transparency of the deposited layers. Scattering measurements showed that the fraction of diffuse reflection and transmission is negligible, so only direct R-T spectra of ZnO:Al on glass are presented here (Fig. 6). Furthermore, a typical fit obtained by application of the single-layer multi-oscillator model is included in the upper graph as an example. The mean square error of this fit is $4.6 \cdot 10^{-3}$.
In the VIS-NIR region a mean transparency around 85% was achieved. In the UV the transparency is limited by band-to-band excitation, according to the bandgap of ZnO of 3.4 eV (≈360 nm) [26]. For longer wavelengths the absorbance is determined by free carrier absorption according to Drude theory. Since the wavelength of plasma resonance λ_P is proportional to $n^{-1/2}$, a shift of λ_P to shorter wavelengths with increasing carrier density is observed (see also Fig. 3). The latter shift is pronounced in the spectra for different N_{DEZ}/N_{TMA}. Here, the IR absorption is also strongly influenced by the mobility. A higher mobility induces a steeper transition into Drude absorption, i.e. the transmission in the NIR should decrease faster. This feature can be seen, too.
Taking the spectra of the sample deposited at 225°C with $N_{DEZ} / N_{TMA} = 20:1$, the complex dielectric function ε was determined using the software LCalc [27] which fits a multi-oscillator model to the reflectance and transmittance spectra:

$$\varepsilon = 1 + \sum_i \frac{A_i}{\omega_{0,i}^2 - \omega^2 - i\beta_i\omega}$$

Here, A_i denotes the strength, $\omega_{0,i}$ the resonance frequency and β_i the damping coefficient of oscillator i. Fig. 7 shows the corresponding refractive index N and absorption coefficient α. While N declines monotonically from 2.02 at 350 nm to 0.86 at 2500 nm, α shows the expected strong increase at 360 nm due to band-to-band excitation and a slow one in the IR spectral region caused by Drude absorption.

3.3. Structural characterization

The following discussion of the structural properties is restricted to ZnO:Al films deposited at 225°C with N_{DEZ} / N_{TMA} = 20:1 since these deposition conditions seem to be most suitable for a-Si:H/c-Si heterojunction devices (see above).
This investigation includes XRD, SEM and AFM measurements. The XRD measurement (Fig. 8) was performed in the Θ-2Θ geometry and shows the hexagonal ZnO structure of the layers. It reveals a dominating (100) peak at 2Θ = 31.9°, meaning that the film grows preferably with the a-axis perpendicular to the substrate. This behavior has also been observed by other authors for ZnO:Al prepared by ALD within this deposition regime [29,30,31].
The SEM image (Fig. 9) of the same sample exhibits "wedge-shaped" [28] crystallites 100 to 200 nm long and only a few nm thick.
For determination of surface roughness a layer prepared with the same parameters was fabricated on a flat Si wafer with a RMS roughness of 0.3 nm. An AFM measurement (not shown here) of the topography yields a film RMS roughness of about 3 nm.

3.4. Contact measurements

In order to examine whether the atomic layer deposited ZnO:Al (225°C, 20:1) forms ohmic or Schottky-type contacts on p- and n-type a-Si:H, simple test structures were fabricated as shown in Fig. 10 (inset). Silicon substrates of the same conductivity type like the examined amorphous silicon layer were used to obtain a low series resistance for the measurement. Here, a high doping density (> 10^{18} cm^{-3}) of the substrates leads to ohmic behavior at the a-Si:H/c-Si contact.
The measured I-V characteristics are shown in Fig. 10. While the test device on p-doped a-Si:H exhibits a linear ohmic trend, the same structure on n-doped a-Si:H shows a non-linear curve. The symmetry with respect to the current axis is due to the symmetry of the test structure.
The latter curve can be interpreted using simple Schottky theory. Thus, on an n-type semiconductor with electron affinity χ, two scenarios are expected, depending on the work function Φ_M of the contact metal:

1. $\Phi_M - (\chi + E_C - E_F) > 0$: depletion of carriers at the junction, non-linear contact.
2. $\Phi_M - (\chi + E_C - E_F) \leq 0$: accumulation of carriers at the junction, ohmic contact.

The measurement corresponds to a series connection of such contacts with opposite directions, both being either of the depleted or the accumulated type, respectively. Fig. 11 shows numerical calculations of the possible situations that were performed using the software AFORS-HET [32]. Three different characteristics are depicted. The broken line (concave for positive voltages) can be expected if barriers are formed and the contacts get depleted. Otherwise, if electrons accumulate at the ZnO:Al/a-Si:H(n), two different characteristics can occur, depending on the dopant density in the amorphous silicon. For sufficiently high n-doping (here: $E_F = E_C - 250$ meV) a linear, ohmic behaviour is expected (solid line). In contrast, weak n-doping (here: $E_F = E_C - 450$ meV) results in a non-linear curve being convex for positive voltages, which is due to the strong influence of carrier injection at low voltages (dotted line). Since our contact measurement on n-type a-Si:H yields the last-mentioned characteristic (which a depleted contact would never do), we conclude that our ZnO:Al/a-Si:H(n) contacts are accumulated. Yet the doping of the a-Si:H(n) is so low that after accumulation at the contact the amorphous silicon bulk is partially depleted. By applying a voltage, electrons are injected into the depleted bulk, leading to a more and more decreased resistivity and hence to the measured characteristic.

3.5. Solar cells

To get an efficient nanostructured silicon heterojunction solar cell, simple planar ZnO:Al/a-Si:H(p)/c-Si(n)/Cr devices without metallic front grid were prepared first. The thickness of the amorphous silicon emitter amounted to ~24 nm. The ZnO:Al was deposited at 225°C with $N_{DEZ} / N_{TMA} = 20:1$ and has a rather high thickness of 500 nm to reach a reasonably low series resistance. Cell definition was done by applying a resist and etching back the 500 nm thick ZnO:Al layer in diluted HF. Fig. 12 shows the illuminated (AM1.5 spectrum, 1000 W/m²) I-V characteristic of such a solar cell with an active area of about 12.3 mm².
The cell exhibits an excellent rectification and reaches an open circuit voltage (V_{OC}) of about 620 mV. The relatively low short-circuit current density (j_{SC}) of 21 mA/cm² is a consequence of light absorption in the thick ZnO:Al film and the amorphous emitter. The absence of an AR coating and a back surface field (BSF) decreases j_{sc} as well.
Finally, we prepared first silicon heterojunction solar cells on two different nanostructures: wet-chemically etched (Fig. 13 a,b,c) and VLS grown (Fig. 13 d) Si nanowires. While (a) shows the pure etched Si nanostructure, (b) and (c) illustrate the good conformal and homogenous growth of the atomic layer deposited ZnO:Al film. The arrow in (c) indicates the cross-sectional view on a single Si nanowire from which it becomes clear that the nanowires are fully coated down to the substrate bottom, despite the high aspect ratio.
Hence, it could be shown that it is possible to provide conformal transparent front electrodes to nanostructured silicon solar cells by applying an atomic layer deposition of ZnO:Al.

4. Conclusion

This work analysed ZnO:Al thin films prepared by ALD from precursors diethylzinc (DEZ), trimethylaluminium (TMA) and water with regard to the fabrication of transparent front electrodes on nanostructure silicon heterojunction solar cells.
The dependence of the most important electrical (ρ, μ, *n*) and optical film parameters on the deposition conditions was examined and discussed in detail. Optimal film properties can be acquired at a N_{DEZ} / N_{TMA} of 20:1 and at deposition temperatures below 250°C, which is compatible with the a-Si:H emitter. The resistivity and the mean transparency amount to about $1.2 \cdot 10^{-3}$ Ωcm and 85%, respectively. Furthermore, the complex dielectric function was determined applying a multi-oscillator model to the transmittance and reflectance spectra. The structural layer properties were analyzed by XRD, AFM and SEM.
It was shown that the ZnO:Al films form ohmic contacts to both n- and p-type a-Si:H and are suitable for silicon heterojunction solar cells. Finally, the conformal layer growth on Si nanowire structures with exceptionally high aspect ratio was demonstrated.
A comprehensive report on the first completely fabricated nanostructure silicon heterojunction solar cells is also published in this journal [33]. These cells reached a record efficiency of 7.3%.

Acknowledgements

The authors acknowledge the financial support by the European Commission in the projects SiNAPS (contract 257856) and NanoPV (contract 246331).

References

1. G. Beaucarne, Silicon thin film solar cells, Adv. Optoelectron. 2007 (2007) 36970.
2. A. M. Morales, C. M. Lieber, A Laser Ablation Method for the Synthesis of Crystalline Semiconductor Nanowires, Science 279 (1998) 208-211.

3. T. Stelzner, M. Pietsch, G. Andrä, F. Falk, E. Ose, S. Christiansen, Silicon nanowire-based solar cells, Nanotechnology 19 (2008) 295203.
4. V. A. Sivakov, G. Brönstrup, B. Pecz, A. Berger, G. Z. Radnoczi, M. Krause, S. H. Christiansen, Realization of Vertical and Zigzag Single Crystalline Silicon Nanowire Architectures, J. Phys. Chem. C, 114-9 (2010) 3798–3803.
5. G. Zhengyu, W. Zhiming, Z. Anyuan, J. Jing, Z. Guodong, J. Yadong, Fabrication of black silicon materials by wet etching and characterization, Proc. SPIE 7658 (2010) 76584S-76584S-7.
6. H. Jansen, M. de Boer, R. Legtenberg, M. Elwenspoek, The black silicon method: a universal method for determining the parameter setting of a fluorine-based reactive ion etcher in deep silicon trench etching with profile control, J. Micromech. Microeng. 5 (1995) 115-120.
7. S. Olibet, E. Vallat-Sauvain, C. Ballif, Model for a-Si:H/c-Si interface recombination based on the amphoteric nature of silicon dangling bonds, Phys. Rev. B 76 (2007) 035326.
8. V. Lujala, J. Skarp, M. Tammenmaa, T. Suntola, Atomic layer epitaxy growth of doped zinc oxide thin films from organometals, Appl. Surf. Sci. 82/83 (1994) 34-40.
9. J. W. Elam, G. Xiong, C. Y. Han, H. H. Wang, J. P. Birrell, U. Welp, J. N. Hryn, M. J. Pellin, T. F. Baumann, J. F. Poco, J. H. Satcher Jr., Atomic Layer Deposition for the Conformal Coating of Nanoporous Materials, J. Nanomater. 2006 (2006) 64501.
10. N. P. Dasgupta, S. Neubert, W. Lee, O. Trejo, J.-R. Lee, F. B. Prinz, Atomic Layer Deposition of Al-doped ZnO Films: Effect of Grain Orientation on Conductivity, Chem. Mater. 22 (2010) 4769–4775.
11. C. H. Ahn, H. Kim, H. K. Cho, Deposition of Al doped ZnO layers with various electrical types by atomic layer deposition, Thin Solid Films 519 (2010) 747–750.
12. A.W. Ott, J. W. Klaus, J. M. Johnson, S. M. George, Al_2O_3 thin film growth on Si(100) using binary reaction sequence chemistry, Thin Solid Films 292 (1997) 135-144.
13. R. L. Puurunen, Surface chemistry of atomic layer deposition: A case study for the trimethylaluminium/water process, J. Appl. Phys. 97 (2005) 121301.
14. L. Niinistö, J. Päiväsaari, J. Niinistö, M. Putkonen, M. Nieminen, Advanced electronic and optoelectronic materials by Atomic Layer Deposition: An overview with special emphasis on recent progress in processing of high-k dielectrics and other oxide materials, phys. stat. sol. (a) 201 (2004), 1443-1452.
15. H. Makino, A. Miyake, T. Yamada, N. Yamamoto, T. Yamamoto, Influence of substrate temperature and Zn-precursors on atomic layer deposition of polycrystalline ZnO films on glass, Thin Solid Films 517 (2009), 3138-3142.
16. H. L. Hartnagel, A. L. Dawar, A. K. Jain, C. Jagadish, Semiconducting transparent thin films, first ed., Institute of Physics Publishing, Bristol and Philadelphia, 1995.
17. J. Hu, R. G. Gordon, Textured aluminium-doped zinc oxide thin films from atmospheric pressure chemical-vapor deposition, J. Appl. Phys. 71 (1992), 880-890.
18. B. Szyszka, Transparent and conductive aluminium doped zinc oxide films prepared by mid-frequency reactive magnetron sputtering, Thin Solid Films 351 (1999), 164-169.
19. Z. L. Pei, C. Sun, M. H. Tan, J. Q. Xiao, D. H. Guan, Optical and electrical properties of direct-current magnetron sputtered ZnO:Al films, J. Appl. Phys. 90 (2001), 3432-3436.
20. H. Ohmi, K. Yasutake, Y. Hamaoka, H. Kakiuchi, Metal induced hydrogen effusion from amorphous silicon, Appl. Phys. Lett. 91 (2007) 241901.

21. H. J. Yang, K.-S. Ji, J. Choi, H. M. Lee, Annealing effect on surface passivation of a-Si:H/c-Si interface in terms of crystalline volume fraction, Curr. Appl. Phys. 10 (2010) S375–S378.
22. S. De Wolf, M. Kondo, Abruptness of a-Si:H/c-Si interface revealed by carrier lifetime measurements, Appl. Phys. Lett. 90 (2007) 042111.
23. S. De Wolf, M. Kondo, Boron-doped a-Si:H/c-Si interface passivation: Degradation mechanism, Appl. Phys. Lett., 91 (2007) 112109.
24. F. Ruske, Deposition and Properties of TCOs, in: W. van Sark, L. Korte, F. Roca (Eds.), Physics and Technology of Amorphous-Crystalline Heterostructure Silicon Solar Cells, Springer, Berlin / Heidelberg, 2012, pp. 301-331.
25. B. Szyszka, Magnetron Sputtering of ZnO Films, in: K. Ellmer, A. Klein, B. Rech (Eds.), Transparent Conductive Zinc Oxide – Basics and Applications in Thin Film Solar Cells, Springer, Berlin / Heidelberg, 2008, pp. 187-235.
26. W. Martienssen, H. Warlimont (Eds.), Springer Handbook of Condensed Matter and Materials Data, Springer, Berlin / Heidelberg, 2005.
27. O. Stenzel, S. Wilbrandt, K. Friedrich, N. Kaiser, Realistische Modellierung der NIR/VIS/UV-optischen Konstanten dünner optischer Schichten im Rahmen des Oszillatormodells, Vak. Forsch. Prax. 21-5 (2009) 15-23.
28. H. Saarenpää, T. Niemi, A. Tukiainen, H. Lemmetyinen, N. Tkachenko, Aluminium doped zinc oxide films grown by atomic layer deposition for organic photovoltaic devices, Sol. Energ. Mat. Sol. Cells 94 (2010) 1379–1383.
29. J. Y. Kim, Y.-J. Choi, H.-H.-Park, S. Golledge, D. C. Johnson, Effective atomic layer deposition procedure for Al-dopant distribution in ZnO thin films, J. Vac. Sci. Technol. A 28-5 (2010) 1111-1114.
30. J. W. Elam, D. Routkevitch, S. M. George, Properties of ZnO/Al2O3 Alloy Films Grown Using Atomic Layer Deposition Techniques, Journal of the Electrochemical Society 150-6 (2003) G339-G347.
31. P. Banerjee, W.-J. Lee, K.-R. Bae, S. B. Lee, G. W. Rubloff, Structural, electrical and optical properties of atomic layer deposition Al-doped ZnO films, J. Appl. Phys. 108 (2010) 043504.
32. R. Stangl, J. Haschke, C. Leendertz, Numerical Simulation of Solar Cells and Solar Cell Characterization Methods: the Open-Source on Demand Program AFORS-HET, in R. D. Rugescu (Ed.), SolarEnergy, InTech Open Access Publisher, 2010, ISBN 978-953-307-052-0, pp. 319-352.
33. G. Jia, M. Steglich, I. Sill, F. Falk, Core-shell heterojunction solar cells on silicon nanowire arrays, Sol. Energ. Mat. Sol. Cells 96 (2012), 226-230.

Figures

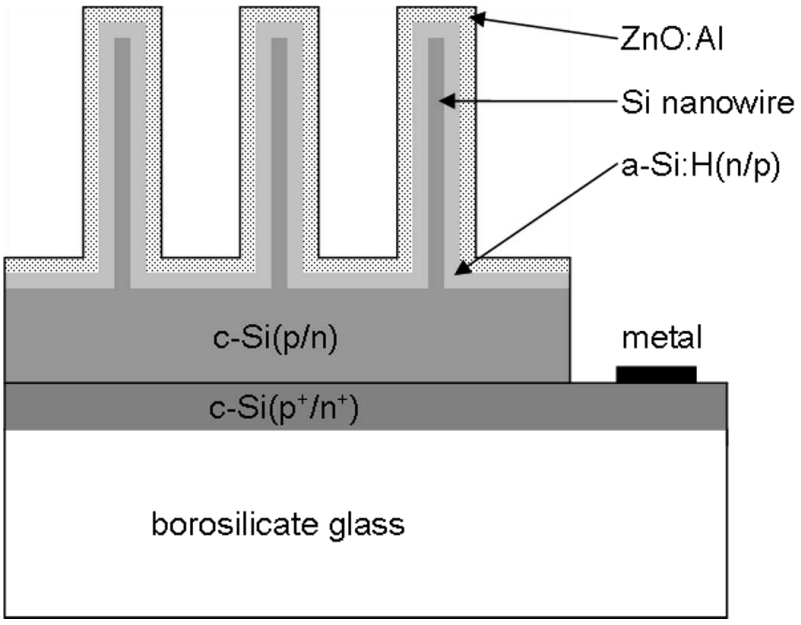

Fig. 1. Thin film nanowire silicon heterojunction solar cell.

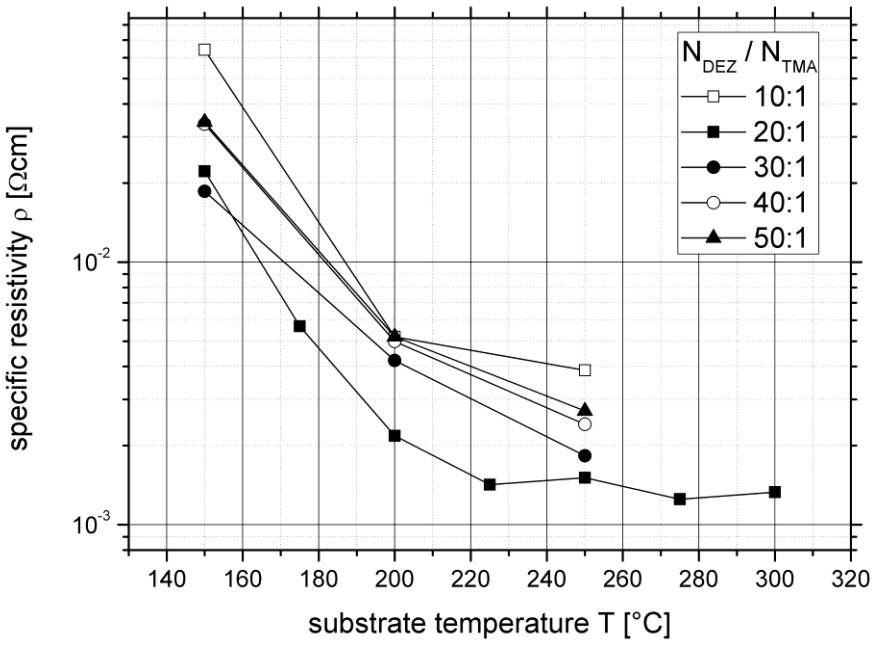

Fig. 2. Resistivity of atomic layer deposited ZnO:Al layers for different substrate temperatures and DEZ-to-TMA ratios.

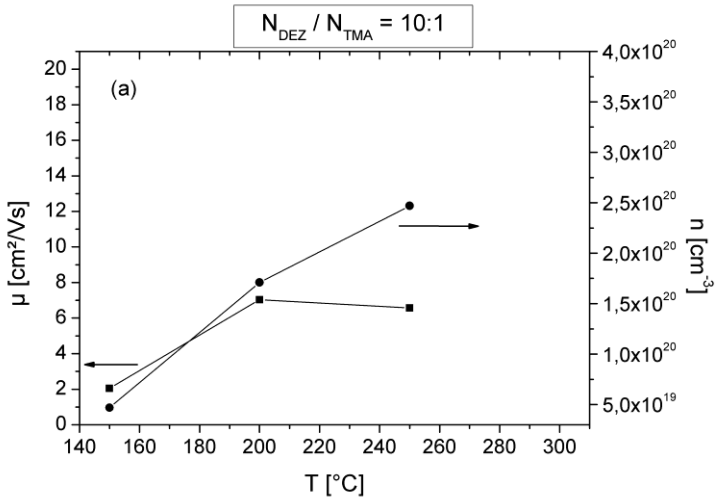

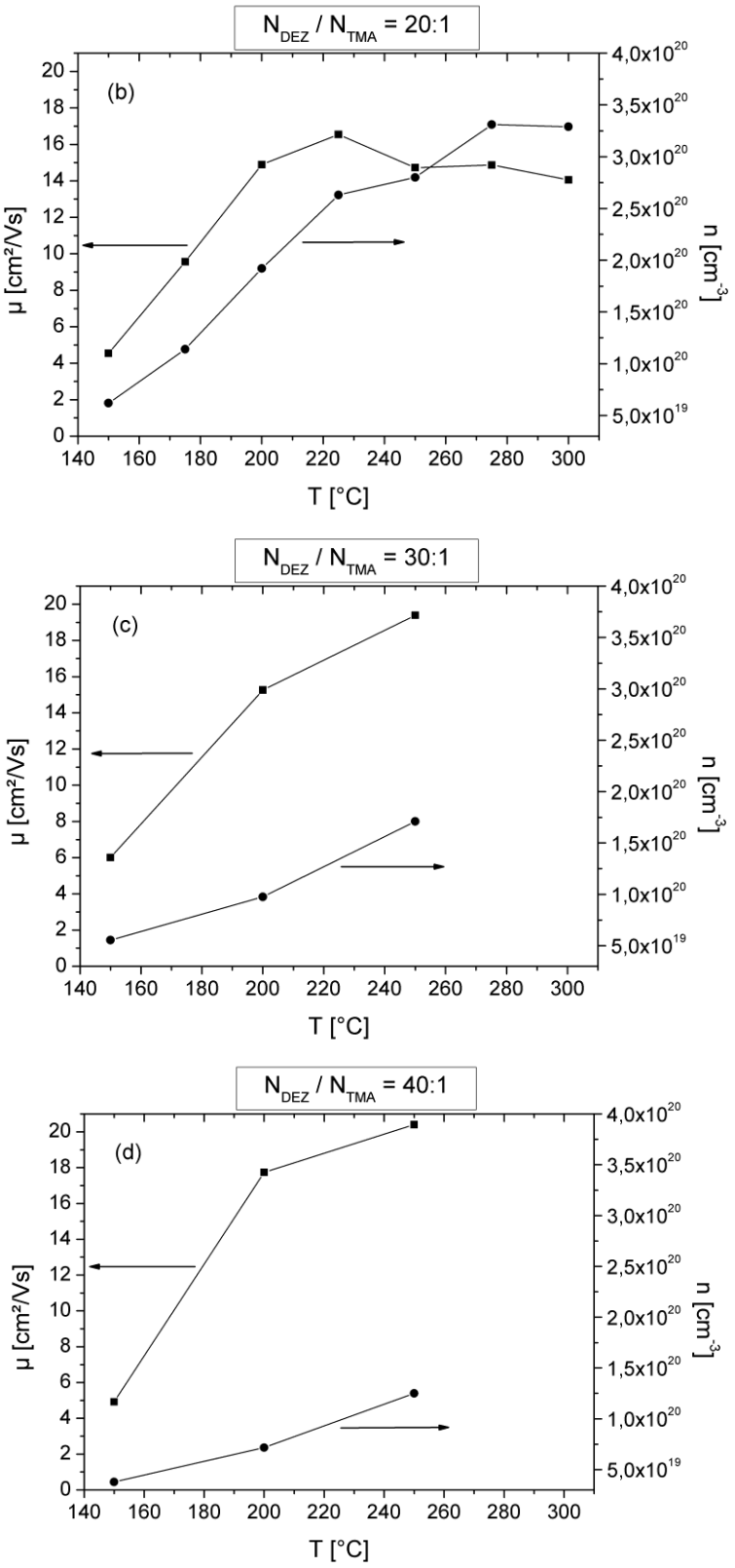

Fig. 3. Mobility μ and carrier density *n* for films prepared at different ALD conditions.

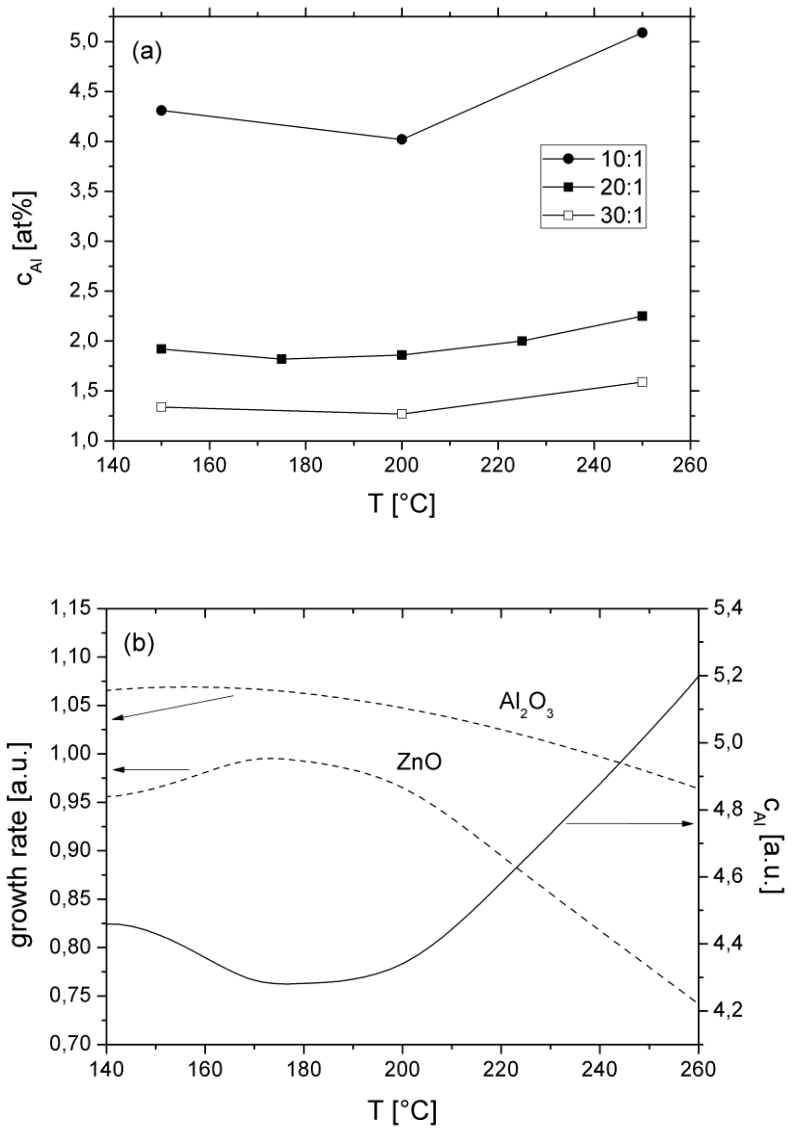

Fig. 4. Al concentration for different ALD conditions, as deduced from EDS (a) and schematic explanation of the concentration dips around 175-200°C (b).

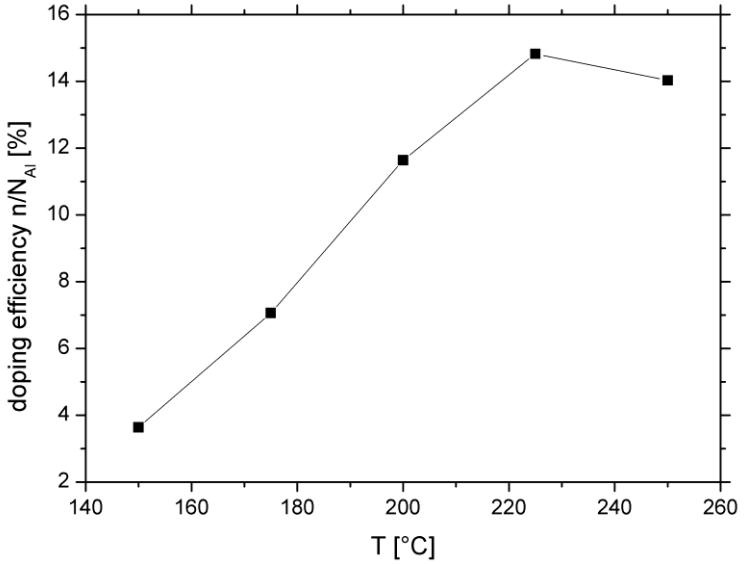

Fig. 5. Doping efficiency n/n_{Al} for N_{DEZ} / N_{TMA} = 20:1.

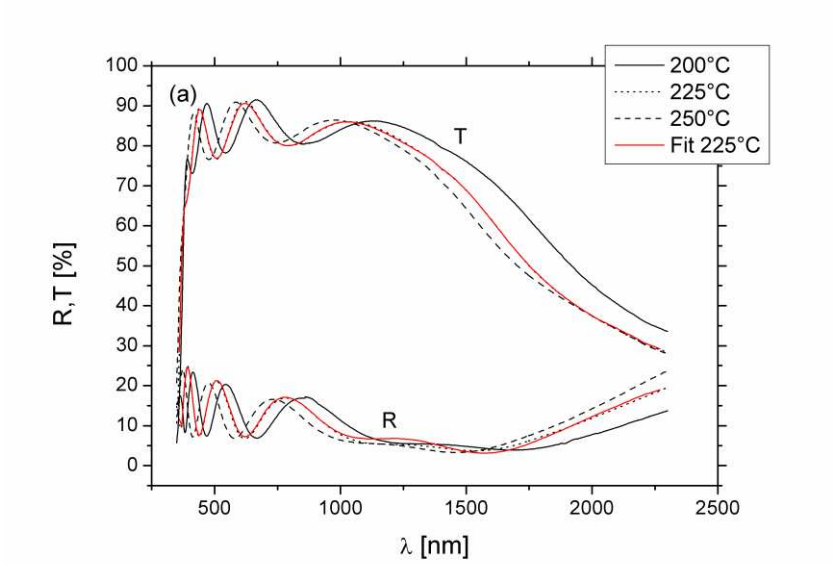

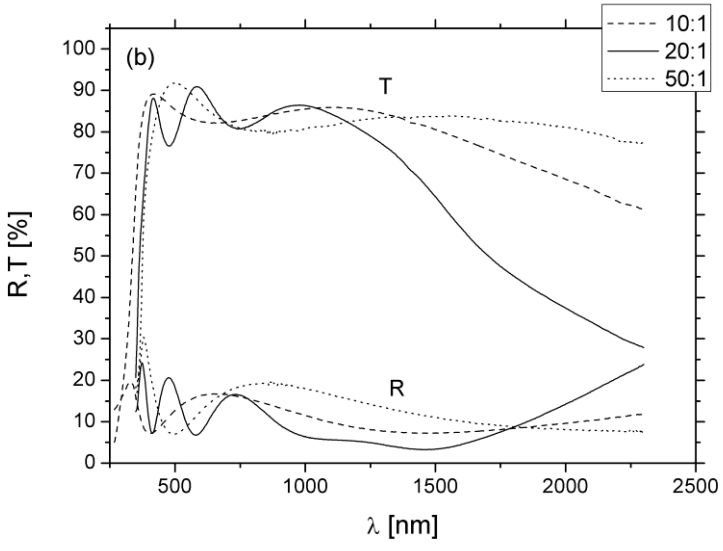

Fig. 6. Transmittance and reflectance spectra of ZnO:Al layers on glass for different deposition temperatures at a constant DEZ-to-TMA ratio of 20:1 (a) and for different N_{DEZ} / N_{TMA} at T = 250°C (b). The shown example fit in (a) is nearly identical to the corresponding measured spectra.

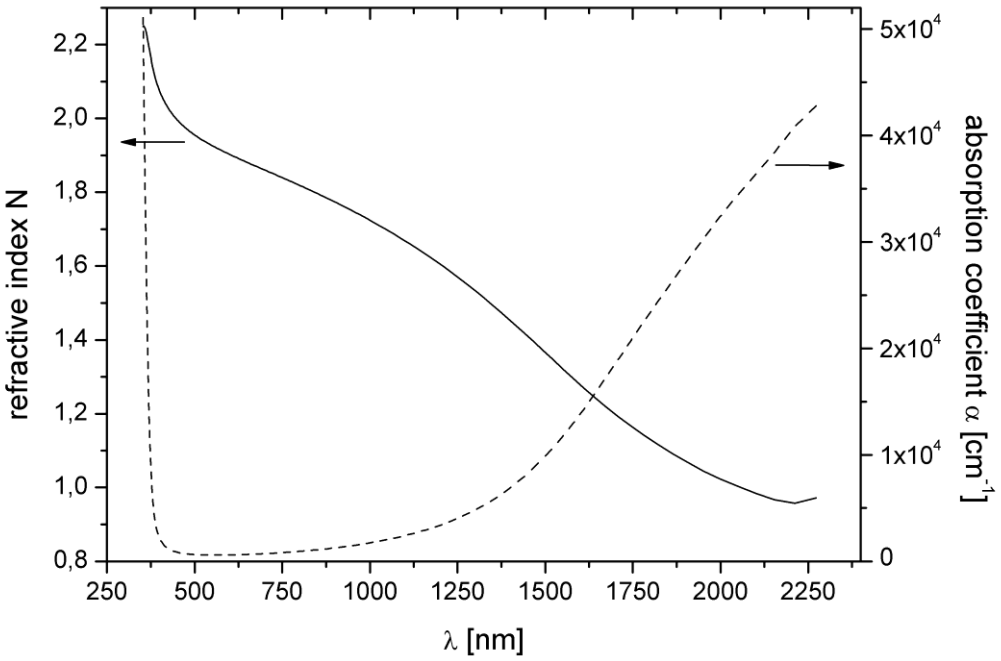

Fig. 7. Refractive index *N* and absorption coefficient α for the (225°C, 20:1) sample.

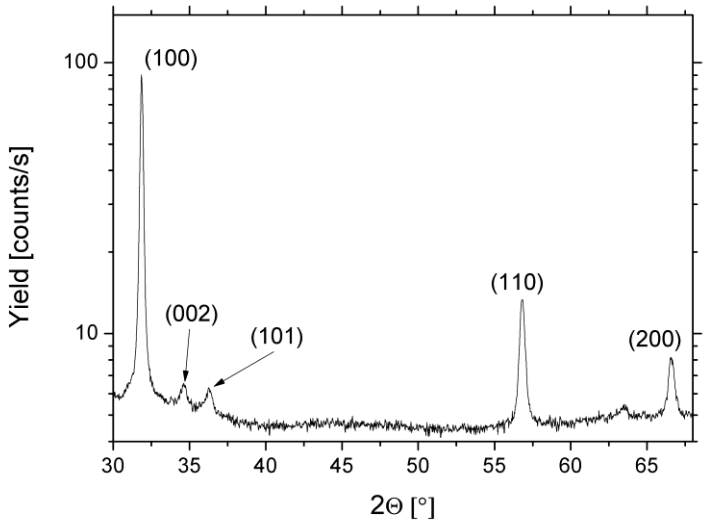

Fig. 8. XRD spectrum of the (225°C, 20:1) sample.

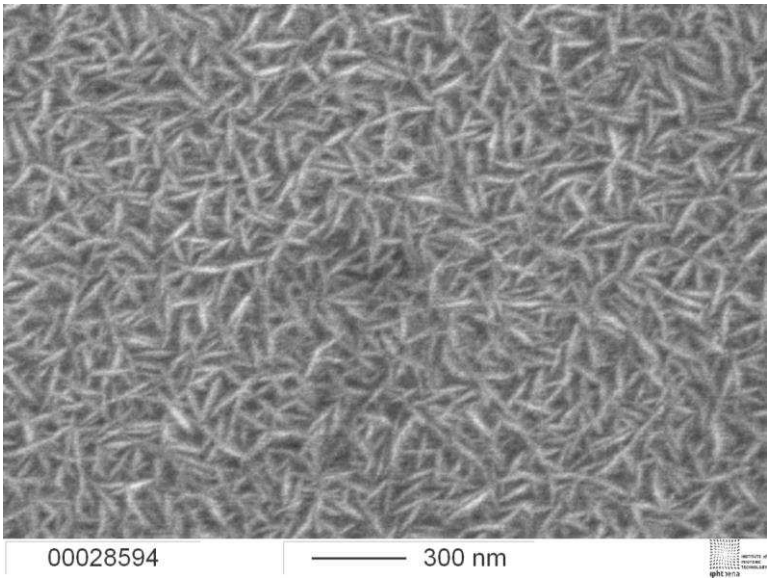

Fig. 9. SEM image of the (225°C, 20:1) sample.

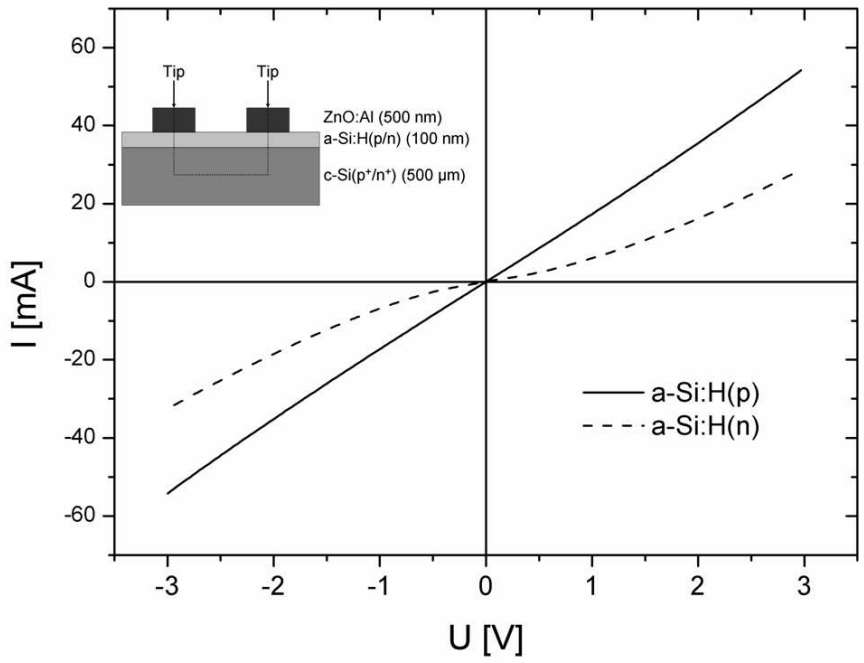

Fig. 10. I-V characteristics of the ZnO:Al/a-Si:H(p)/c-Si(p^+) (solid curve) and the the ZnO:Al/a-Si:H(n)/c-Si(n^+) (dashed curve) test structure. The inset schematically shows the test structure.

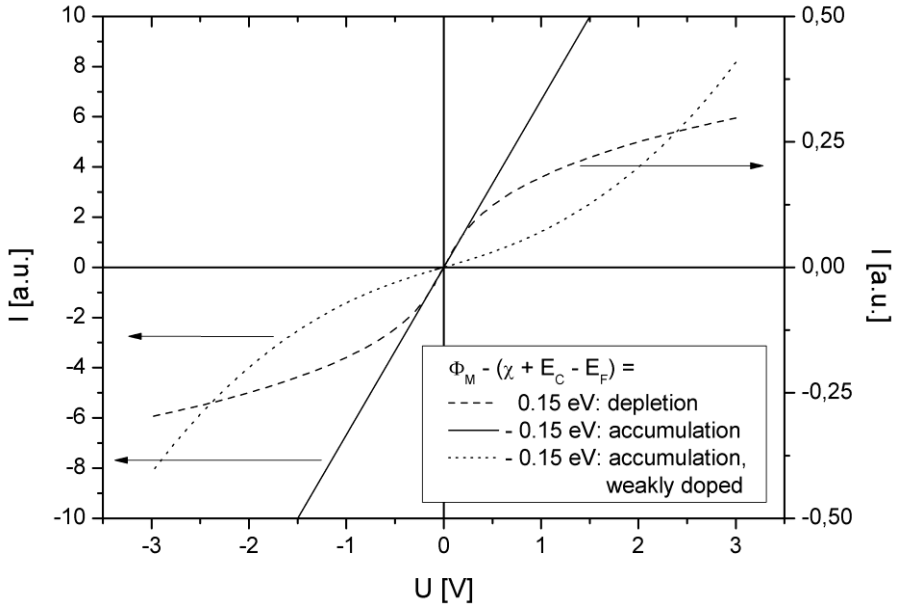

Fig. 11. Simulated I-V characteristics for different work functions of the ZnO:Al layer.

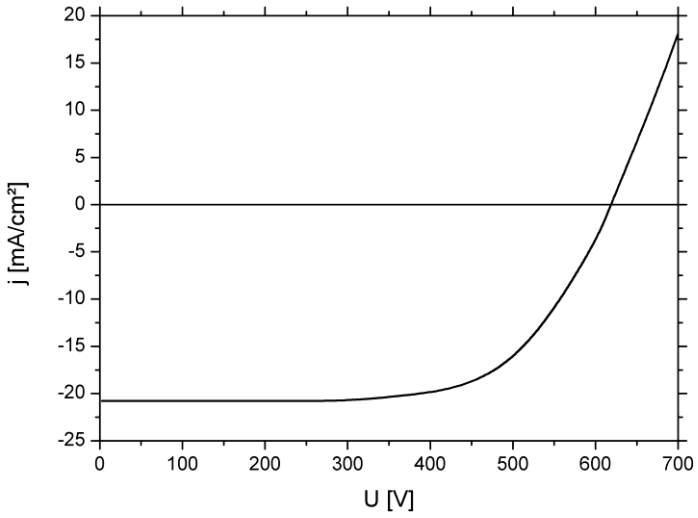

Fig. 12. I-V characteristic of ZnO:Al/a-Si:H(p)/c-Si(n)/Cr solar cell under AM1.5 illumination.

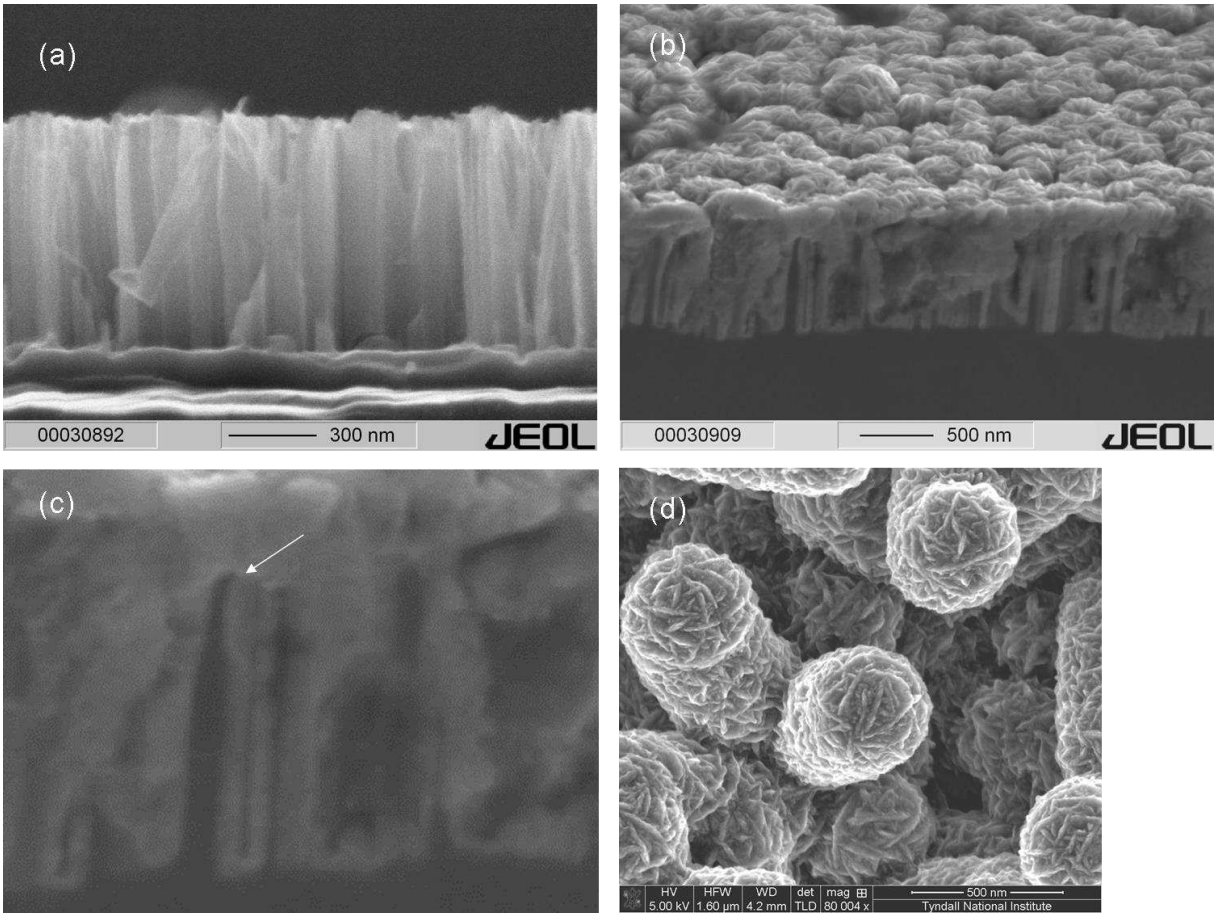

Fig. 13. Cross-section SEM images of etched Si nanowires without (a) and with (b), (c) a-Si:H/ZnO:Al, and SEM image of VLS grown (d) Si nanowires with a-Si:H/ZnO:Al.